THE JOURNAL OF PHYSICAL CHEMISTRY A

Article

pubs.acs.org/JPCA

Structural Trends in Monoboronyl Compounds: Analysis of the Interaction of Second-Row Elements with BO

Published as part of The Journal of Physical Chemistry virtual special issue "Manuel Yáñez and Otilia Mó Festschrift".

Pilar Redondo, Víctor M. Rayón, Carmen Barrientos, and Antonio Largo*

Departamento de Química Física y Química Inorgánica, Facultad de Ciencias, Universidad de Valladolid Campus Miguel Delibes, Paseo de Belén 7, 47011 Valladolid, Spain

Supporting Information

ABSTRACT: A theoretical study of the monoboronyl compounds of second-row elements, [XBO] (X = Na, Si, P, S, Cl), has been carried out. It is observed that the preference for the XBO arrangement is higher when moving to the right of the period. In the case of sodium monoboronyl three minima were characterized, all lying rather close in energy: linear NaBO, linear NaOB, and an L-shaped structure. Linear NaBO and the L-shaped structure are nearly isoenergetic, whereas linear NaOB is located 2.11 kcal/mol above linear NaBO. The barrier for the conversion of the L-shaped structure into linear NaBO is about 5.1 kcal/mol, suggesting that both species could be potential targets for experimental detection. For silicon monoboronyl, two minima, linear SiBO and linear SiOB, are found, the latter lying about 13 kcal/mol above SiBO. The barrier for the isomerization of SiOB into SiBO is estimated to be 11.4 kcal/mol. For phosphorus, sulfur, and chlorine monoboronyls the linear XBO isomer is clearly the most stable one, and the barriers for the conversion into XOB species are relatively high, suggesting that quite likely the linear XBO isomer should be the main experimental target. All studied monoboronyls are relatively stable, with dissociation energies increasing from left to right of the second-row (69.8 kcal/mol for NaBO and 118.98 kcal/mol for ClBO). An analysis of the bonding for second-row monoboronyls has been carried out, emphasizing the different characteristics of the X−B and X−O bonds along the second row.

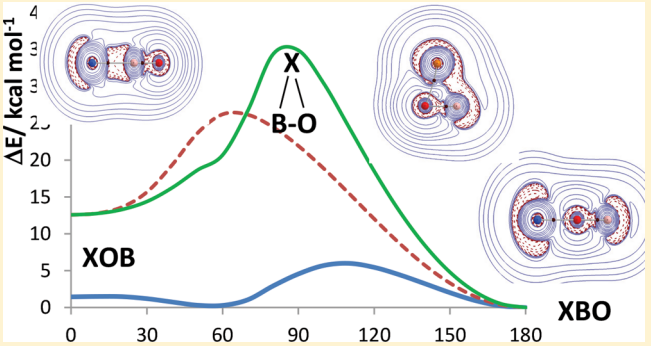

1. INTRODUCTION

Boronyl, BO, has received increased attention in recent years. It was suggested by Ehlers et al.[1] as a potential ligand, given its similarity with the well-known isoelectronic analogue cyanide, CN, and its close similarity with CO. In a recent account Zhai et al.[2] suggested that boronyl is a robust ligand, exhibiting a strong B−O multiple bond, which could lead potentially to a rich chemistry. However, its use in synthetic chemistry has been hindered by the high reactivity of free monomeric BO, making difficult the preparation of complexes incorporating boronyl ligands. It was not until very recently that Braunschweig et al.[3,4] successfully synthesized platinum oxoboryl complexes, followed by the generation of a trinuclear complex of ruthenium capped by a triply bridging oxoboryl ligand by Kaneko et al.[5] In addition, other metal−boronyl compounds, such as $AuBO^-$, Au_2BO^-, Au_3BO^-, and $Au(BO)_2^-$, have been generated and studied by spectroscopic techniques in the gas phase.[6,7] Boronyl compounds with nonmetals, such as boron or diborene, have also been generated.[8,9] Organic compounds containing boronyl are also known. CH_3BO was studied spectroscopically[10,11] a few years ago, whereas very recently several boronyl compounds were generated through bimolecular reactions of boronyl with unsaturated hydrocarbons by Kaiser and Balucani.[12] The latter work paves the way for generating organo boronyl monomers.

From the theoretical side, several works[13−23] have been devoted to the prediction of the molecular structure and properties of different complexes of transition metals. These studies provided clues about the behavior of boronyl as a ligand with different metals. Less extensive is the literature about metallic monoboronyls, despite their possible intrinsic interest and relationship with the isoelectronic cyanide/isocyanide analogues. Theoretical studies have been carried out for LiBO,[24] $ScBO^+$,[25] XBO (X = Li, Na, K),[26] RBO (R = H, F, Cl, CH_3),[27] and PtBO and PdBO.[28] We have recently performed a theoretical study of metallic monoboronyl compounds,[29] selecting different types of representative metals, namely, Mg (s-type), Al (p-type), and the group 11 metals Cu,

Received: October 23, 2017
Revised: December 11, 2017
Published: December 11, 2017

DOI: 10.1021/acs.jpca.7b10482
J. Phys. Chem. A XXXX, XXX, XXX−XXX

Ag, and Au (d-type). In the present work we provide a theoretical study of monoboronyls of the rest of second-row elements (metals and nonmetals): Na, Si, P, S, and Cl. There are two main objectives in the present work. First, predictions for the molecular structure and spectroscopic parameters of monoboronyl compounds will be made to guide a possible experimental observation of these species. Second, structural trends along the second row will be discussed and compared to their cyanide analogues.

2. THEORETICAL METHODS

Explorations of the [XBO] potential energy surfaces, X being a second-row element (Na, Si, P, S, Cl), were performed at the coupled cluster level with single and double substitutions (CCSD) employing the all-electron Dunning's correlated consistent triple-ζ basis set augmented with diffuse and polarization functions, denoted as aug-cc-pVTZ.[30,31] Geometry optimizations for the stationary points on the different potential energy surfaces were then carried out at the CCSD and CCSD(T) levels, where the latter stands for a perturbative inclusion of triple excitations.[32] Harmonic vibrational frequencies were computed at the CCSD/aug-cc-pVTZ level, allowing us to check the nature of stationary points according to the number of imaginary frequencies (one imaginary frequency for transition states, and all frequencies real for true minima). For open-shell systems spin contamination was found to be negligible for linear or quasi-linear geometries. Nevertheless, for nonlinear structures (mainly transition states) significant spin contamination was observed when unrestricted Hartree−Fock wave functions were employed. Therefore, to avoid this problem, restricted open-shell Hartree−Fock reference wave functions were employed for the coupled cluster calculations unless otherwise specified. Nevertheless, no significant differences are found between restricted and unrestricted calculations for most structures.

The T1 diagnostic[33] was applied to check the validity of the single-reference based coupled cluster theory. The T1 values for the different minima found in the present study are summarized in Table S1 of the Supporting Information. As can be seen in all cases, low values are found, suggesting that the coupled cluster calculations are reliable enough.

To obtain more reliable predictions, the geometrical parameters and electronic energies were improved through a composite procedure[34−36] for the different stable structures. In addition to the geometry optimizations at the CCSD(T)/aug-cc-pVTZ level, optimizations at the CCSD(T) level with the quadruple-ζ basis set aug-cc-pVQZ were also carried out. The complete basis set limit (CBS) was then estimated through the n^{-3} extrapolation formula[37] for the case n = 3, 4. In the case of sodium we observed an erratic behavior when employing the aug-cc-pVQZ, very similar to that observed in the case of magnesium.[29] Therefore, for the [NaBO] system no extrapolation was performed, and the CCSD(T)/aug-cc-pVTZ results were employed.

Two further corrections have been applied to geometrical parameters and electronic energies. First, core−valence (CV) effects were computed as the difference between a calculation including all electrons and a frozen-core approach at the CCSD level with the aug-cc-pCVTZ basis set,[31,38] which is especially designed to incorporate core−valence correlation. In this way, the core−valence corrections for geometrical parameters (r) and energy (E) are estimated as

$$\Delta r/\Delta E(\mathrm{CV}) = r/E(\mathrm{CCSD\text{-}full/aug\text{-}cc\text{-}pCVTZ}) - r/E(\mathrm{CCSD/aug\text{-}cc\text{-}pCVTZ}) \quad (1)$$

Second, scalar relativistic (Rel) effects were considered through the use of Douglas−Kroll-type[39−41] calculations employing the aug-cc-pVTZ-DK basis set. The difference between calculations at the CCSD level employing the aug-cc-pVTZ-DK and aug-cc-pVTZ basis sets provides an estimate of relativistic corrections:

$$\Delta r/\Delta E(\mathrm{Rel}) = r/E(\mathrm{CCSD\text{-}DK/aug\text{-}cc\text{-}pVTZ\text{-}DK}) - r/E(\mathrm{CCSD/aug\text{-}cc\text{-}pVTZ}) \quad (2)$$

Taking into account these two corrections, and assuming additivity, the final geometrical parameters and energies for Na species are obtained through the composite procedure as

$$r/E = r/E(\mathrm{CCSD(T)/aug\text{-}cc\text{-}pVTZ}) + \Delta r/\Delta E(\mathrm{CV}) + \Delta r/\Delta E(\mathrm{Rel}) \qquad \mathrm{Na} \quad (3)$$

whereas for the rest of second-row elements the different properties are obtained in a similar way, but extrapolating to the CBS limit

$$r/E = r/E(\mathrm{CBS}) + \Delta r/\Delta E(\mathrm{CV}) + \Delta r/\Delta E(\mathrm{Rel}) \qquad \mathrm{Si, P, S, Cl} \quad (4)$$

This procedure has proven to provide excellent agreement with the experimental results for the only species observed spectroscopically so far, namely, ClBO, as demonstrated in our previous work (see Table S2 of ref 29).

Core−valence and relativistic corrections for some representative structures (linear XBO and XOB species) are given in the present work as Supporting Information (Table S2). The contributions of core−valence and relativistic corrections to the relative energies are generally quite small. However, the corrections to the geometrical parameters are not negligible, especially the core−valence corrections. In fact, for the only species observed experimentally, ClBO, the agreement between the theoretical rotational constant (5202.2 MH) (including core−valence and relativistic corrections) and the experimental value (5202.3960 MHz) is very good.[29] Neglecting core−valence and relativistic corrections leads to a deviation of more than 20 MHz from the experimental value. Therefore, we think that it is worthwhile to include these corrections to obtain more reliable predictions.

Spin−orbit corrections were computed for open-shell states employing CASSCF calculations with the aug-cc-pVTZ basis set, taking 10 orbitals as active space and the appropriate number of electrons for each case (N = 9, 10, 11 for Si, P, and S systems, respectively). Illustrative results are given in Table S3 of the Supporting Information. As can be seen, no relevant contributions to the relative energies between the different isomers are found.

All calculations were carried out with the Gaussian 09[42] and CFOUR[43] packages. To get further information about the bonding in the studied systems, a topological analysis of the electronic density within the framework of the quantum theory of atoms in molecules (QTAIM)[44] was carried out. At this end, the AIMAll package[45] was employed.

DOI: 10.1021/acs.jpca.7b10482
J. Phys. Chem. A XXXX, XXX, XXX−XXX

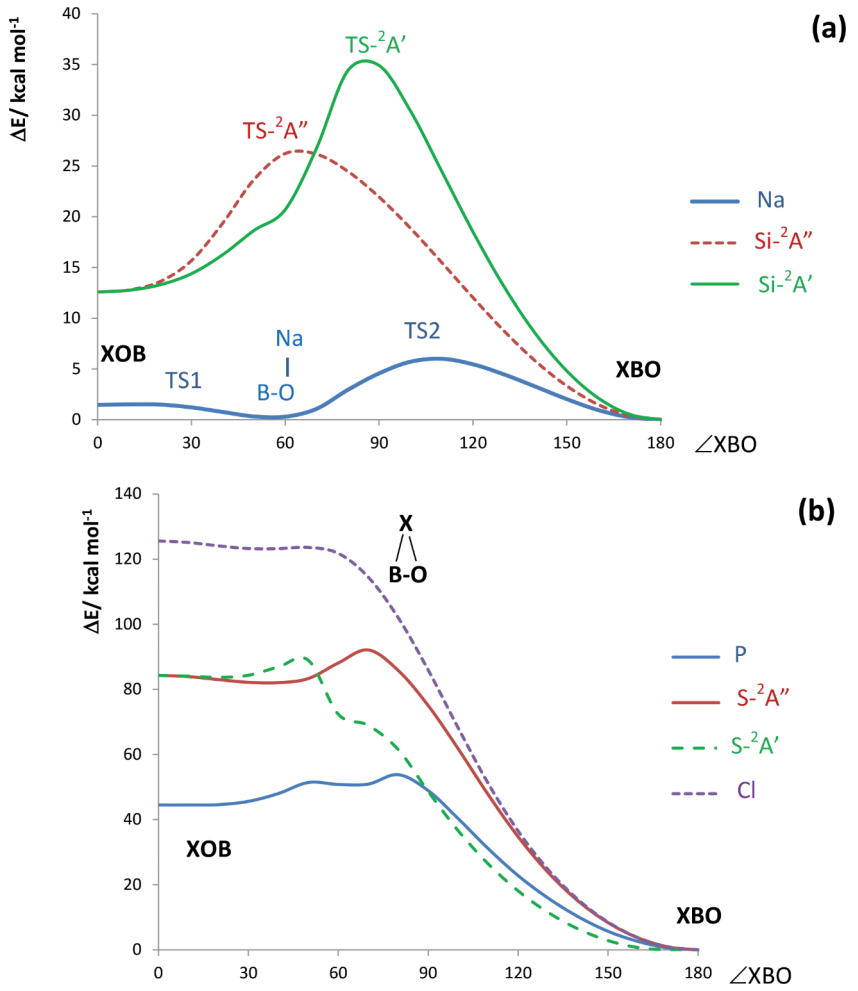

Figure 1. Scans obtained through optimizations at different fixed ∠XBO angles. The relative energies (taking the XBO isomer as reference) at the CCSD/aug-cc-pVTZ level of theory are given in kcal/mol: (a) X = Na, Si; (b) X = P, S, Cl.

Table 1. Structural Data and Relative Energies (kcal/mol) for the Minima and Transition States on the [NaBO] Potential Surface[a]

species	r(Na−B)	r(B−O)	r(Na−O)	∠NaBO	∠NaOB	A_e (A_o)	B_e (B_o)	C_e(C_o)	μ	ΔE
NaBO($^1\Sigma^+$)	2.3986	1.2263					3855.8 (3844.8)		10.659	0.0
NaOB($^1\Sigma^+$)		1.2598	1.9772				5782.9 (5819.8)		11.570	2.11
NaOB(^{1}A′)	2.4981	1.2517	2.1118	57.65	92.30	54211.2 (55844.3)	8340.9 (8232.3)	7228.7 (7128.7)	8.871	0.26
TS1(NaOB($^1\Sigma^+$)−NaOB(^{1}A′))	3.2048	1.2622	1.9890	12.19	160.11					1.76
TS2(NaOB(^{1}A′)−NaBO($^1\Sigma^+$))	2.3251	1.2348	2.9467	107.77	48.71					5.36

[a]Internuclear distances, r (Å), bond angles (deg), and rotational constants (MHz) were obtained at the CCSD(T)/aug-cc-pVTZ level. For the minima, core−valence and relativistic corrections were also included through a composite procedure. Dipole moments (D) for the minima were computed at the CCSD/aug-cc-pVTZ level on the CCSD(T)/aug-cc-pVTZ optimized geometries.

3. RESULTS AND DISCUSSION

Detailed scans of the [XBO] potential energy surfaces (X being Na, Si, P, S, and Cl) were carried out at several levels of theory. In Figure 1 we represent the energy obtained after optimizations of the X−B and B−O distances at fixed ∠XBO angles at the (restricted) CCSD/aug-cc-pVTZ level against the ∠XBO angles. The two extremes in the graphic, the angles 0° and 180°, represent XOB and XBO isomers, respectively. Different behaviors are observed, and therefore we will discuss each system separately.

[NaBO]. For Na, a rather flat potential surface is found. Three different minima were characterized at the CCSD level: linear NaBO ($^1\Sigma^+$ electronic state), linear NaOB ($^1\Sigma^+$ electronic state), and a nonlinear structure (^{1}A′). The bond angles in the nonlinear species at that level of theory are 57.2° (∠NaBO) and 87.2° (∠NaOB), suggesting that this species could be described more properly as an L-type structure rather than a T-shaped one. We also characterized the two transition states connecting the three minima. The observed behavior for the [NaBO] system is similar to that found for the analogue

DOI: 10.1021/acs.jpca.7b10482
J. Phys. Chem. A XXXX, XXX, XXX−XXX

Table 2. Harmonic, ω, and Anharmonic, ν (in Parentheses) Vibrational Frequencies (cm^{-1}) for [NaBO] Species Evaluated at the CCSD/aug-cc-pVTZ Level[a]

	NaBO($^1\Sigma^+$)		NaOB($^1\Sigma^+$)		NaOB($^1A'$)		TS1	TS2
mode	ω	I	ω	I	ω	I	ω	ω
bending	188 (187)	14.59 (14.55)	63 (17)	0.00 (0.01)	154 (136)	45.44 (42.61)	73i	176 i
Na−B/Na−O stretching	322 (306)	43.83 (37.32)	447 (433)	67.17 (64.8)	388 (385)	50.43 (49.24)	442	386
B−O stretching	1869 (1847)	94.7 (92.26)	1661 (1638)	229.38 (212.18)	1684 (1661)	132.49 (131.56)	1660	1812

[a]IR intensities (I, km/mol) are also given for predicted minima.

[NaCN] system, exhibiting a floppy potential surface, characteristic of polytopic systems.[46] In fact, theoretical works[47,48] found also three minima, predicting a T-shaped structure as the global [NaCN] minimum, in agreement with the experimental evidence.[49,50] This T-shaped structure has been observed in the interstellar medium.[49] The behavior of the [NaBO] system also resembles the [LiBO] one.[24] Papakondylis and Mavridis[24] found also a polytopic behavior in [LiBO] with three minima on the potential energy surface: linear LiBO, linear LiOB and a bent structure.

The geometrical parameters, spectroscopic constants, and relative energies for the [NaBO] species are given in Table 1, whereas the vibrational frequencies and IR intensities are provided in Table 2. A relatively long Na−B bond distance is observed for the linear NaBO isomer, whereas the Na−O distance for the linear NaOB species is much shorter. However, the B−O bond distance is shorter for the NaBO species (1.2263 Å) and closer to the distance observed in the isolated BO molecule (1.2043 Å at the same level of theory). This may suggest that the bonding through the boron atom (where the unpaired electron in BO is mainly localized) has a smaller effect in the strength of the B−O bond than the bonding through the oxygen atom. It is also worth pointing out that the corrected value for the ∠NaOB angle (including core−valence and relativistic effects) in the nonlinear species is 92.3°, further supporting that it could be an L-type structure.

The relative energies shown in Table 1 reflect the characteristics of a rather flat potential energy surface. According to these values, the linear NaBO species and the nonlinear structure are nearly isoenergetic, with the former lying just 0.26 kcal/mol lower in energy. This makes it difficult to draw a final conclusion. However, there are some clues that may help. In fact, the nonlinear species is found below the linear NaBO isomer at the CCSD/aug-cc-pVTZ level by 0.28 kcal/mol. Incorporating the triple substitutions in the CCSD treatment places linear NaBO 0.1 kcal/mol below the nonlinear species, and the final relative energy prediction of −0.26 kcal/mol is reached after incorporation of core−valence and relativistic corrections. Therefore, it seems that improving the level of calculation slightly favors the linear NaBO structure. In any case, it seems that both species should be very close in energy. The estimated barrier for the isomerization of C_s-NaOB into linear NaBO is 5.16 kcal/mol, and it should not be discarded that both species could eventually be observed experimentally. There are some subtle but important differences between the [NaBO] system and its isoelectronic [NaCN] one. For the latter the nonlinear species is found to be the global minimum, with linear NaNC and linear NaCN lying 2.21 and 2.70 kcal/mol, respectively, higher in energy according to the theoretical predictions.[48] The nonlinear structure is the only one observed experimentally.[49,50] The barriers for isomerization into the nonlinear species are 0.04 and 1.25 kcal/mol, respectively for linear NaNC and NaCN. Such small barriers probably imply that, even if any of the linear species is eventually formed, surely it would isomerize into the nonlinear global minimum. That could be certainly the case also for linear NaOB. The relative energy for linear NaOB at the CCSD(T)/aug-cc-pVTZ+ZPE level is 1.91 kcal/mol, which is already slightly higher than the relative energy of TS1 (1.76 kcal/mol) at the same level of theory, suggesting that quite likely the linear NaOB should not be a true minimum at higher levels of theory. On the CCSD/aug-cc-pVTZ potential surface linear NaOB is found as a minimum, of course with an electronic energy lower than TS1, but upon addition of the ZPE correction, the relative order is reversed and linear NaOB is placed slightly above TS1. Its very low bending frequency, 63 cm^{-1} (Table 2), also points to a very facile conversion into the nonlinear species. However, the energy barrier existing between NaBO and the nonlinear species, around 5 kcal/mol, could be high enough to prevent isomerization under appropriate experimental conditions. Therefore, it seems that these two species are nearly isoenergetic and both could be possible targets for experimental observation. It seems that for [LiBO] the isomerization barrier could be even higher. Papakondylis and Mavridis[24] report an energy barrier for the Li−OB → Li−BO isomerization of 10.5 kcal/mol, nearly twice the one found for [NaBO].

All [NaBO] species show very high dipole moments (from 8.871 to 11.570 D) reflecting a high ionic character. Being closed-shell species, and the linear structures not subject to Renner−Teller splitting, we were able to successfully apply a second-order perturbative treatment to account for anharmonic corrections in the vibrational frequencies and vibration−rotation interactions. Therefore, B_o (A_o and C_o for the nonlinear species) values for rotational constants are given in Table 1, whereas both harmonic and anharmonic vibrational frequencies and IR intensities are collected in Table 2. Very different rotational constants are observed for NaBO and NaOB. As can be seen in Table 2, the anharmonic frequencies are slightly lower than the harmonic ones, the most noticeable difference observed for the bending motion in linear NaOB. The harmonic value is rather low, 63 cm^{-1}, and the anharmonic frequency even lower, taking a value of just 17 cm^{-1}. These values confirm the low stability of this species, suggesting a facile conversion into the nonlinear structure. For both NaBO and NaOB($^1A'$) the IR spectrum should be dominated by the B−O stretching.

[SiBO]. In the case of [SiBO] only two minima were found, as can be seen in Figure 1. Both minima correspond to the linear isomers, SiBO and SiOB, and have $^2\Pi$ electronic ground states. Thus, a very similar behavior to that found for the isoelectronic [SiCN] system is found. For the latter system different theoretical works[48,51,52] have shown that both SiCN and SiNC are linear molecules, silicon isocyanide lying less than 2 kcal/mol above silicon cyanide. The rotational spectra of both SiCN and SiNC were experimentally observed[53,54] by

DOI: 10.1021/acs.jpca.7b10482
J. Phys. Chem. A XXXX, XXX, XXX−XXX

Table 3. Structural Data and Relative Energies (kcal/mol) for the Minima and Transition States on the [SiBO] Potential Surface[a]

species	r(Si−B)	r(B−O)	r(Si−O)	∠SiBO	∠SiOB	B_e	μ	ΔE
SiBO($^2\Pi$)	2.0154	1.2081				4512.3	3.411	0.0
SiOB($^2\Pi$)		1.2924	1.6731			6529.6	2.971	13.15
TS1($^2A'$)	2.1114	1.2442	2.3720	85.85	62.60			34.43
TS2($^2A''$)	2.207	1.2664	1.9340	60.72	84.46			24.59

[a]Internuclear distances, r (Å), bond angles (deg), and equilibrium rotational constants (MHz) were obtained at the CCSD(T)/aug-cc-pVTZ level. For the minima CBS, core−valence and relativistic corrections were also included through a composite procedure. Dipole moments (D) for the minima were computed at the CCSD/aug-cc-pVTZ level on the CCSD(T)/aug-cc-pVTZ optimized geometries.

Fourier transform microwave and millimeter-wave absorption spectroscopy. Furthermore, both species have been detected in an astronomical source.[55,56]

The geometrical parameters, spectroscopic constants, and relative energies obtained for the [SiBO] species are given in Table 3. The corresponding harmonic vibrational frequencies and IR intensities are provided in Table 4. No attempt was made in this case to obtain the anharmonic corrections to vibrational frequencies and IR intensities, because both SiBO and SiOB are linear molecules subject to Renner−Teller splitting, given their $^2\Pi$ electronic state. It can be readily seen in Table 3 that the B−O distance in SiBO, namely, 1.2081 Å, is very similar to that found for isolated BO, whereas the Si−B bond distance is rather large, about 2.0154 Å. It seems that in SiBO the BO unit is unaffected by the silicon atom. However, in the case of SiOB the B−O distance is lengthened compared to that found in isolated BO, taking a value larger than 1.29 Å, whereas the Si−O bond distance is relatively short, 1.6731 Å. Therefore, there is a large difference between the Si−B and Si−O distances found in each isomer. This is in contrast with the bond distances found for the isoelectronic pair SiCN/SiNC. Senent et al.[48] and Richardson et al.[52] found a Si−C bond length around 1.85 Å for linear SiCN and a Si−O bond distance of 1.74 Å in the case of linear SiOB. As a consequence of the rather different bond lengths, the corresponding rotational constants are very different for SiBO (4512.3 MHz) and SiOB (6529.6 MHz). It is interesting to note that both SiBO and SiOB have noticeable dipole moments, 3.411 and 2.971 D, but much smaller than those exhibited by the [NaBO] species.

Table 4. Harmonic Vibrational Frequencies (ω, cm^{-1}) for [SiBO] Species Evaluated at the CCSD/aug-cc-pVTZ Level[a]

	SiBO($^2\Pi$)		SiOB($^2\Pi$)		TS1($^2A'$) TS2($^2A''$)	
mode	ω	I	ω	I	ω	ω
bending	188	14.59	63	0.01	439 i	281 i
Si−B/Si−O stretching	322	43.83	447	67.17	546	476
B−O stretching	1869	94.7	1661	229.38	1727	1625

[a]IR intensities (I, km/mol) are also given for predicted minima.

The theoretical calculations predict that SiBO should be the global minimum, thus favoring bonding of silicon to the less electronegative atom of the B/O pair. This result is similar to the observation of SiCN as the global minimum for the [SiCN] system. Nevertheless, SiOB is found to lie about 13 kcal/mol above SiBO, an energy difference much larger than that found between SiNC and SiCN, namely less than 2 kcal/mol.[48,51,52]

In C_s symmetry the $^2\Pi$ electronic state splits into $^2A'$ and $^2A''$ electronic states, depending on the orbital (in-plane and out-of-plane, respectively) where the unpaired electron is allocated. The corresponding potential energy surfaces, for different ∠SiBO angles, are shown in Figure 1. The shape of the potential surfaces confirms that there are no other minima apart from the linear species. As in the case of [SiCN],[52] two transition states are found for the SiOB → SiBO isomerization process, one for each potential surface, TS1($^2A'$) and TS2($^2A''$). The corresponding geometrical parameters of the transition states are also provided in Table 3. It is readily seen that TS1($^2A'$) has a slightly longer Si−O distance than TS2($^2A''$), whereas the B−O distances are slightly longer in TS2($^2A''$). The ∠SiBO angle (85.85) illustrates that TS1($^2A'$) is closer to the SiBO species, whereas TS2($^2A''$) appears at a smaller ∠SiBO angle (60.72°) and it is located closer to SiOB. It is found at all levels that TS2($^2A''$) is located clearly lower in energy than TS1($^2A'$). This behavior parallels that found for the [SiCN] system and, in a similar way as suggested by Richardson et al.,[52] is probably due to the possibility of interaction of a lone pair of oxygen with the empty a′ orbital in TS2($^2A''$). The main difference with the situation found in the

Table 5. Structural Data and Relative Energies (kcal/mol) for the Minima and Transition States on the [PBO] Potential Surface[a]

species	r(P−B)	r(B−O)	r(P−O)	∠PBO	∠POB	A_e	B_e	C_e	μ	ΔE
PBO($^3\Sigma^-$)	1.8717	1.2063					4767.9		2.989	0.00
POB($^3\Sigma^-$)		1.2930	1.6385				6431.5		2.852	46.44
POB($^3A''$)		1.2928	1.6376		178.01	8307918.3	6415.0	6405.5	2.768	46.45
PBO($^3A''$)	1.9067	1.3012	1.8142	65.76	73.41	45769.9	11585.1	9245.3	0.719	48.05
TS1(POB($^3A''$)−PBO($^3A''$))	2.2369	1.7675	1.3110	52.16	91.99					51.67
TS2(PBO($^3A''$)−PBO($^3\Sigma^-$))	1.9701	2.1463	1.2571	80.06	64.71					51.58

[a]Internuclear distances, r (Å), bond angles (deg), and equilibrium rotational constants (MHz) were obtained at the CCSD(T)/aug-cc-pVTZ level. For the minima CBS, core−valence and relativistic corrections were also included through a composite procedure. Dipole moments (D) for the minima were computed at the CCSD/aug-cc-pVTZ level on the CCSD(T)/aug-cc-pVTZ optimized geometries.

DOI: 10.1021/acs.jpca.7b10482
J. Phys. Chem. A XXXX, XXX, XXX−XXX

Table 6. Harmonic Vibrational Frequencies (ω, cm^{-1}) for [PBO] Species Evaluated at the CCSD/aug-cc-pVTZ Level[a]

	PBO($^3\Sigma^-$)		POB($^3\Sigma^-$)	POB($^3A''$)		PBO($^3A''$)		TS1 TS2	
mode	ω	I	ω	ω	I	ω	I	ω	ω
bending	329	23.97	38 i	57	3.41	480	27.05	373 i	457 i
P−B/P−O stretching	550	5.45	687	694	77.24	503	37.20	580	619
P−O stretching	1957	105.85	1454	1439	850.99	1407	38.53	1380	1599

[a]IR intensities (I, km/mol) are also given for predicted minima.

[SiCN] system[52] is that in the present case the energy barrier is much higher on the $^2A'$ potential surface, whereas for [SiCN] the barriers on each surface differ in less than 1 kcal/mol.[52]

The energetic results suggest that SiBO is clearly favored over SiOB, with an energy difference of 13 kcal/mol. However, the energy barrier for the SiOB → SiBO isomerization is about 11.4 kcal/mol on the more favorable $^2A''$ potential surface. Therefore, SiOB could retain its identity and cannot be discarded as a possible target for experimental observation. The data shown in Table 4 show that both SiBO and SiOB IR spectra should be dominated mainly by the B−O stretching. The corresponding frequency for such mode is predicted to be considerably higher for SiBO (1869 cm^{-1}) than for SiOB (1661 cm^{-1}).

[PBO]. Three minima have been located on the potential energy surface of [PBO]. The scan can be seen in Figure 1b, and in this case the UHF wave function was employed as reference for the subsequent CCSD calculations. The most relevant geometrical parameters, spectroscopic constants, and relative energies of these isomers have been collected in Table 5 whereas vibrational frequencies and IR intensities are shown in Table 6. The lowest energy minimum is linear PBO, which has a $^3\Sigma^-$ electronic ground state. The isoelectronic molecule PCN also has a $^3\Sigma^-$ ground state as anticipated by theoretical studies[57,58] and confirmed by its pure rotational spectrum.[59] Besides the PBO linear isomer, two bent structures (C_s symmetry) have been identified: a quasi-linear POB isomer and a T-shaped structure. Both have $^3A''$ ground states. Location of a quasi-linear isomer in the PES of [PBO] is due to the fact that linear POB ($^3\Sigma^-$) has a small imaginary frequency (38i cm^{-1}) at the CCSD level associated with the bending normal mode. The calculated ∠POB angle in the quasi-linear structure (178°) departs actually very little from its linear value. Furthermore, after extrapolation at the CCSD(T) level and incorporation of the core−valence and relativistic corrections, the linear and quasi-linear POB species are nearly isoenergetic. This fact reflects the very flat form of the PES in the surroundings of the linear POB linear isomer. In any case, if either linear or nonlinear, this isomer lies 46.45 kcal/mol above the lowest lying linear PBO isomer. However, the T-shaped isomer lies 1.60 kcal/mol above the quasi-linear POB one and 48.05 kcal/mol above linear PBO. The two transition structures with C_s symmetry located on the CCSD PES show small barriers for the conversion of the quasi-linear isomer with the T-shaped structure (5.12 kcal/mol) and of the T-shaped isomer with linear PBO (3.53 kcal/mol). On the other side, the energy barrier required to reach the T-shaped structure from PBO is, as expected, very large: 51.58 kcal/mol. Thus, the relatively complex potential energy surface of [PBO] suggests that, even if three minima are found, quite likely the clear target for experimental observation should be linear PBO.

Table 5 shows the most relevant geometrical parameters of the three isomers of [PBO]. Linear PBO has a P−B bond length of 1.8717 Å, much shorter than the Si−B bond length in SiBO, 2.3986 Å. This is striking because similar bond distances were found in the isoelectronic cyanide analogs: Si−CN (1.844 Å) and P−CN (1.732 Å). The B−O bond distance (1.2063 Å) is very close to the isolated B−O value (1.2043 Å), showing that in PBO the BO moiety is only slightly perturbed by the phosphorus atom. However, the P−O distance in linear POB is 1.6385 Å (the Si−O distance is 1.6731 Å for SiOB, Table 3), about 0.2 Å shorter than P−B bond distance in PBO. Quasi-linear POB($^3A''$) displays geometrical parameters very similar to those of linear POB($^3\Sigma^-$), Table 5. This is expected because quasi-linear POB($^3A''$) is only slightly distorted from the linear arrangement (∠POB = 178°). However, T-shaped PBO has similar P−B and P−O bond distances, 1.9067 and 1.8142 Å, respectively, and a BO distance of 1.3012 Å. The dipole moments of PBO and quasi-linear POB($^3A''$) are relatively large (2.989 and 2.768 D, respectively) whereas T-shaped PBO shows a much smaller moment, namely, 0.719 D.

As commented above, quasi-linear POB($^3A''$) and T-shaped PBO lie more than 46 kcal/mol above linear PBO. This follows the expected trend through the periodic row of increasing energy differences between both isomers. Also, this probably makes PBO as the sole target for experimental observation. The vibrational frequencies and infrared intensities of PBO are

Table 7. Structural Data and Relative Energies (kcal/mol) for the Minima and Transition States on the [SBO] Potential Surface[a]

species	r(S−B)	r(B−O)	r(S−O)	∠OSB	∠SOB	A_e	B_e	C_e	μ	ΔE
SBO($^2\Pi$)	1.7503	1.2093					5125.3		2.759	0.00
SOB($^2\Pi$)		1.2952	1.6212				6431.8		2.649	83.61
SOB(C_s,$^2A''$)		1.3391	1.6814		100.42	58545.8	9442.7	8113.9	1.769	80.96
SOB(C_s,$^2A'$)		1.3022	1.6356		148.00	304142.7	6801.8	6655.7	2.362	83.25
TS($^2A''$)	2.0343	1.2918	1.9395	67.086	75.05					86.34
TS($^2A'$)		1.3075	1.7541		100.14					87.11

[a]Internuclear distances, r (Å), bond angles (deg), and equilibrium rotational constants (MHz) were obtained at the CCSD(T)/aug-cc-pVTZ level. For the minima CBS, core−valence and relativistic corrections were also included through a composite procedure. Dipole moments (D) for the minima were computed at the CCSD/aug-cc-pVTZ level on the CCSD(T)/aug-cc-pVTZ optimized geometries.

DOI: 10.1021/acs.jpca.7b10482
J. Phys. Chem. A XXXX, XXX, XXX−XXX

Table 8. Harmonic Vibrational Frequencies (ω, cm^{-1}) for [SBO] Species Evaluated at the CCSD/aug-cc-pVTZ Level[a]

	SBO($^2\Pi$)		SOB($^2A''$)		SOB($^2A'$)		SOB($^2\Pi$) TS($^2A''$)		TS($^2A'$)
mode	ω	I	ω	I	ω	I	ω	ω	ω
bending	379	27.77	123	3.3	145	5.42	122i	502i	607i
S−B/S−O stretching	635	0.10	763	64.78	719	28.29	696	623	493
B−O stretching	1931	104.7	1284	335.74	1404	622.8	1460	1348	1491

[a]IR intensities (I, km/mol) are also given for predicted minima.

shown in Table 6. The spectra of PBO should be dominated by the B−O stretching with a corresponding frequency of 1957 cm^{-1}.

[SBO]. In the case of the system containing sulfur, [SBO], the linear isomer SBO($^2\Pi$) is a true minimum, whereas linear SOB($^2\Pi$) corresponds to a transition state. The analysis of the scan connecting these two linear structures reported in Figure 1b shows the presence of an angular SOB minimum and a transition state, which connects this minimum with linear SBO, which is clearly the global minimum (located about 80 kcal/mol below the angular structures). The same behavior is found on the two surfaces, $^2A'$ and $^2A''$ surfaces, correlating with the $^2\Pi$ state. We can also see that the potential surface is rather flat in the area close to SOB($^2\Pi$) isomer. However, in the case of the isoelectronic system [SCN] theoretical studies of the potential energy surface[60,61] find a different profile with three minima, two linear, SCN and SNC, and a cyclic structure, and two transition states connecting them.

The geometrical parameters, spectroscopic constants, and relative energies obtained for the [SBO] species are given in Table 7. The corresponding harmonic vibrational frequencies and IR intensities are provided in Table 8. As for the systems [SiBO] and [PBO], no attempt was made in this case to obtain the anharmonic corrections to vibrational frequencies and IR intensities. In Table 7 we can see that if we compare the BO distance in the two linear structures with that of BO ligand, this distance is slightly increased (0.005 Å) when sulfur is bonded through the boron atom whereas in the case of SOB the B−O distance is lengthened by 0.0909 Å. We can also see that the distance S−B is larger than the S−O. These facts indicate that the interaction of sulfur atom through boron has a slight effect on the BO unit. The two angular minima, SOB($^2A''$) and SOB($^2A'$), show an increase in the two distances S−O and B−O respect to the linear structure, SOB($^2\Pi$).

The relative energies given in Table 7 show that the global minimum is clearly the linear isomer SBO ($^2\Pi$), which is located 80.96 kcal/mol below the most stable angular structure, SOB ($^2A''$). We can also see that $^2A''$ and $^2A'$ potential energy surfaces are very close in energy. The minimum and transition state located on the $^2A''$ surface are slightly more stable (energy differences are less than 3 kcal/mol). The isomerization barrier for SOB ($^2A''$, $^2A'$) → SBO ($^2\Pi$) is only 5.38 and 3.86 kcal/mol, respectively. Comparing these results with those reported for the isoelectronic system,[60,61] [SCN], we find that the energy difference between the two isomers increases and the isomerization barrier decreases. Diehr et al.[60] found at the MRCI level that SNC lies 29.7 kcal/mol above SCN, and the isomerization barriers are 27.4 and 32.7 kcal/mol on the $^2A''$ and $^2A'$ potential energy surface, respectively.

The relative energies reported in Table 7 show that SBO is clearly favored over the most stable angular structure SOB ($^2A''$), with an energy difference of 80.96 kcal/mol. In addition, the energy barrier for the SOB ($^2A''$) → SBO ($^2\Pi$) isomerization is only 5.38 kcal/mol, on the more favorable $^2A''$ potential surface. Therefore, SBO seems to be the target for experimental observation. The data for the vibrational frequencies are shown in Table 8, where it can be seen that the IR spectra of SBO should be dominated mainly by the B−O stretching (1931 cm^{-1}).

[ClBO]. This is the only [XBO] species containing a second-row element that has been observed experimentally so far. In particular, different spectroscopic studies[62−65] have characterized linear ClBO. For that reason we employed this species as a test case for validating the theoretical methods employed in our previous study on some metallic monoboronyl compounds,[29] as well as in the present work. A very good agreement between the theoretical vibrational frequencies and rotational constant and the experimental values was observed,[27] lending support to the employment of the theoretical methods. The theoretical results for ClBO can be found in the Supporting Information of ref 27, so in the present work we will just briefly comment on the characteristics of the rest of stationary points.

We have explored the potential energy surface for the [ClBO] system computing the energy at different ∠ClBO angles. The resulting energy profile is shown in Figure 1. It can be seen that the linear ClOB species lies very high in energy, about 124 kcal/mol above linear ClBO. Furthermore, it is found to be a transition state, an observation confirmed by the calculation of vibrational frequencies. Two degenerate imaginary frequencies (188i cm^{-1}) are found for linear ClOB. Following this bending mode a shallow minimum, ClOB($^1A'$), is reached at ∠ClBO angle of 39.37° and ∠ClOB angle of 111.28° (CCSD(T)/aug-cc-pVTZ level). This minimum lies 119.5 kcal/mol above ClBO at the same level of theory. In addition, the transition state for the isomerization into ClBO is located at 120.3 kcal/mol, suggesting that the energy barrier for the isomerization of ClOB($^1A'$) into linear ClBO is 0.8 kcal/mol. Therefore, it seems that this minimum should be quite unstable and should lead eventually to the most stable isomer ClBO or even dissociate into Cl and BO. In fact, spontaneous dissociation seems to be the fate of this species if eventually formed, because it lies 3.68 kcal/mol above the Cl(^2P) + BO($^2\Sigma^+$) limit. For that reason no further details of its structure will be discussed.

Stability of [XBO] Systems. As mentioned before, for [NaBO] there is a small difference in stability among the different isomers. In fact, linear NaBO and the nonlinear species are nearly isoenergetic. For the rest of second-row monoboronyls the preference for the XBO arrangement is more marked as one moves to the right of the second row, as can be seen by analyzing the relative energies shown in the preceding tables. A similar behavior is observed for the isoelectronic [XCN] compounds, but in the case of monoboronyls there seems to be a larger difference in stability between the XBO/XOB isomers than for the XCN/XNC pairs.

DOI: 10.1021/acs.jpca.7b10482
J. Phys. Chem. A XXXX, XXX, XXX−XXX

An interesting property to analyze is the dissociation energy associated with the process XBO/XOB → X + BO. The computed dissociation energies for the different minima characterized in the present work are summarized in Table 9. In all cases the dissociation limits are the ground states of the atoms (Na(^{2}S), Si(^{3}P), P(^{4}S), S(^{3}P), Cl(^{2}P)) and the BO ground state ($^2\Sigma^+$), correlating for all studied systems with the ground electronic states of the [XBO] systems. For Na and Si both XBO and XOB arrangements have moderate dissociation energies, suggesting that the bonding of the second-row element to the BO unit could be strong enough to maintain the identity of the monoboronyl for both connectivities. However, for second-row elements with electronegativities higher than that of boron (P, S, Cl), the dissociation energy of XOB species is very low, suggesting rather unstable structures. Focusing on XBO isomers, which seem to be the most stable ones, it can be seen that dissociation energies tend to increase along the second row from left to right. In all cases, relatively large dissociation energies are found, and especially for SBO and ClBO these values are certainly high, 97.55 and 118.98 kcal/mol, respectively, suggesting the formation of potentially stable compounds. In fact, as mentioned before, the closed-shell species ClBO has been produced in experiments.[62−65]

Table 9. Dissociation Energies (D_0, kcal/mol) of the [XBO] (X = Na, Si, P, S, Cl) Species[a]

species	D_0
NaBO($^1\Sigma^+$)	69.80
NaOB(^{1}A′)	69.71
NaOB($^1\Sigma^+$)	67.90
SiBO($^2\Pi$)	79.24
SiOB($^2\Pi$)	66.37
PBO($^3\Sigma^-$)	78.97
POB(^{3}A″)	34.38
SBO($^2\Pi$)	97.55
SOB(^{2}A″)	18.48
SOB(^{2}A′)	13.37
ClBO($^1\Sigma^+$)	118.98

[a]They were obtained at the extrapolated CCSD(T) level, employing the aug-cc-pVTZ and aug-cc-pVQZ basis sets. Zero-point vibrational energy (ZPVE) corrections are also taken into account at the CCSD/aug-cc-pVTZ level. Dissociation energies correspond to the XBO/XOB → X + BO fragmentation process. Both fragments are in their respective ground states.

Bonding Analysis of [XBO] Systems. To provide further insight into the bonding in [XBO] species, we have employed the natural bond orbital (NBO) formalism[66] and the atoms in molecules (AIM) theory.[31] Some of the main results from the NBO analysis are provided in Table 10, and a summary of the AIM analysis is shown in Table 11.

Table 11. Local Topological Properties[a] (au) of the Electronic Charge Density Distribution Calculated at the Position of the Bond Critical Points for the Different XBO/XOB Species (Level of Calculation CCSD/aug-cc-pVTZ)

species	bond	$\rho(r)$	$\nabla^2\rho(r)$	$\lvert V(r)\rvert/G(r)$	$H(r)$
NaBO($^1\Sigma^+$)	Na−B	0.029	0.117	0.965	0.001
	B−O	0.298	1.852	1.384	−0.288
NaOB(^{1}A′)	Na−O	0.037	0.281	0.875	0.008
	B−O	0.277	1.565	1.402	−0.263
NaOB($^1\Sigma^+$)	Na−O	0.050	0.403	0.914	0.008
	B−O	0.269	1.497	1.400	−0.249
SiBO($^2\Pi$)	Si−B	0.098	0.041	1.865	−0.065
	B−O	0.305	1.979	1.375	−0.297
SiOB($^2\Pi$)	Si−O	0.114	0.825	1.138	−0.033
	B−O	0.227	1.263	1.371	−0.186
PBO($^3\Sigma^-$)	P−B	0.148	−0.316	4.361	−0.113
	B−O	0.306	2.006	1.373	−0.298
PBO(^{3}A″)	P−O	0.118	0.263	1.577	−0.0897
	B−O	0.243	1.204	1.432	−0.228
POB($^3\Sigma^-$)	P−O	0.144	0.723	1.344	−0.095
	B−O	0.219	1.312	1.341	−0.170
SBO($^2\Pi$)	S−B	0.169	−0.290	2.684	−0.178
	B−O	0.304	1.993	1.373	0.296
SOB(^{2}A″)	S−O	0.178	0.106	1.883	−0.227
	B−O	0.223	0.954	1.455	−0.438
SOB($^2\Pi$)	S−O	0.182	0.397	1.661	−0.194
	B−O	0.210	1.366	1.307	−0.151
ClBO($^1\Sigma^+$)	Cl−B	0.170	−0.008	2.012	−0.176
	B−O	0.301	1.976	1.373	−0.295
ClOB(^{1}A′)	Cl−O	0.189	−0.094	2.196	−0.144
	B−O	0.222	0.968	1.450	−0.198
ClOB($^1\Sigma^+$)	Cl−O	0.199	−0.143	2.253	−0.177
	B−O	0.198	1.447	1.264	−0.130

[a]The electronic charge density [$\rho(r)$], the Laplacian [$\nabla^2\rho(r)$], the relationship between the potential energy density $V(r)$ and the Lagrangian form of kinetic energy $G(r)$ and the total energy density $H(r)$.

Table 10. Natural Atomic Charges (q), Bond Order Indices (b), and Populations of the Second-Row Element Valence Orbitals (n_s, n_p, n_d) for the XBO and XOB Species Obtained at the CCSD/aug-cc-pVTZ Level (BO Values Also Given as Reference)

species	q(X)	q(B)	q(O)	b(X−B)	b(B−O)	b(X−O)	n_s(X)	n_p(X)	n_d(X)
NaBO($^1\Sigma^+$)	0.760	0.160	−0.920	0.37	1.59	0.01	0.20	0.04	0.00
SiBO($^2\Pi$)	0.407	0.364	−0.771	0.90	1.71	0.02	1.79	1.72	0.06
PBO($^3\Sigma^-$)	0.193	0.556	−0.749	1.06	1.71	0.01	1.80	2.90	0.08
SBO($^2\Pi$)	0.023	0.708	−0.731	1.18	1.69	0.06	1.80	4.04	0.10
ClBO($^1\Sigma^+$)	−0.126	0.896	−0.770	1.06	1.41	0.00	1.83	5.15	0.11
NaOB($^1\Sigma^+$)	0.975	0.290	−1.265	0.01	1.12	0.01	0.01	0.11	0.00
SiOB($^2\Pi$)	0.776	0.518	−1.294	0.05	0.752	0.37	1.78	1.37	0.05
POB($^3\Sigma^-$)	0.644	0.525	−1.169	0.05	0.746	0.53	1.81	2.44	0.01
SOB($^2\Pi$)	0.507	0.536	−1.043	0.10	0.75	0.67	1.83	3.53	0.08
ClOB($^1\Sigma^+$)	0.358	0.563	−0.921	0.16	0.86	0.68	1.88	4.62	0.04
BO		0.869	−0.869		1.62				

DOI: 10.1021/acs.jpca.7b10482
J. Phys. Chem. A XXXX, XXX, XXX−XXX

Boronyl, BO, has clearly a multiple bond. There is experimental evidence,[67] as well as theoretical studies,[25] suggesting that the boron−oxygen bond in BO can be described as a triple bond. Our NBO analysis[29] is also compatible with a $^{\bullet}B{\equiv}O$: structure. The qualitative picture resulting from the NBO analysis corresponds to two bonds coming from the sharing of unpaired electrons at boron and oxygen atoms (the boron atom being formally in a ^4P state) and a third bond being in fact of a dative nature from oxygen toward the boron atom, in agreement with the pioneering work of Papakondylis and Mavridis on BO and related systems.[24,25] The relatively low value (for a triple bond) of the bond index in BO (1.62) could be due to the large difference in electronegativity between oxygen and boron resulting in a strong polarization of the bonds. As can be seen in Table 10, the bond indices for the B−O bonds in XBO isomers remain close to that of isolated boronyl, reflecting that the B−O bond is only slightly affected by the bonding of the X atom through the unpaired electron at the boron atom in boronyl. However, the B−O bond index is noticeably reduced in XOB isomers, reflecting the weakening of the B−O bond (in accordance with the structural and vibrational frequencies data). In addition, the X−O bond indices for XOB structures are lower than the X−B indices for XBO isomers. This is probably related to the more covalent contribution in the X−B bonding as a consequence of the unpaired electron localized at the boron atom in isolated BO. In both types of isomers the bond indices tend to increase from left to right along the second row, probably as a consequence of the variation in electronegativity, which anticipates more ionic character for less electronegative X elements. It is also worth pointing out that non-negligible values for the X−B bond indices in XOB compounds are observed, especially for the XOB isomers of sulfur and chlorine (0.10 and 0.16, respectively). These bond indices for nonadjacent atoms reflect through-atom antibonding interactions[29,68,69] and are observed for triatomic systems usually when the central atom is more electronegative than the other two atoms.

The NBO atomic charges, q, might provide some clues about the ionic/covalent contributions in the different bonds. Obviously, $q(X)$ decreases from left to right along the second row, following the variation of electronegativity and, as expected, indicating the larger ionic character of X−B and X−O bonds for more electropositive atoms. The larger $q(X)$ values found for XOB isomers than for XBO structures also reflect the difference in electronegativity between the bonded atoms. It is worth pointing out the value of $q(Na) = 0.975$ for NaOB, together with a Na−O bond index of just 0.01, which suggests nearly a complete transfer of an electron from sodium to oxygen approaching a clearly ionic interaction. In all cases the charges of the second-row atoms, as well as the charge at the oxygen atom, are clearly larger for the XOB species than for the XBO ones, suggesting a high degree of ionic character for the X−O bonds. The amounts of charge transfer from the valence 3s orbital are rather similar for both XBO and XOB species, whereas the populations of 3p orbitals are clearly smaller in the XOB structures than in the XBO ones. Therefore, it seems that the extra charge transfer in XOB isomers comes from the 3p orbitals. The role of 3d orbitals is rather limited, although always slightly larger for XBO isomers.

The data from the AIM analysis in Table 11 for the B−O bonds are in accordance with previous theoretical works on monoboronyls[29] and borates.[70] The low values of the electronic charge density, $\rho(r)$, and positive values of its Laplacian, $\nabla^2\rho(r)$, are indicative of a closed-shell interaction, whereas the negative value of the total energy density, $H(r)$, suggests a certain character of covalent interaction. Therefore, as in previous studies,[29,70] the B−O bonds in the present case of second-row monoboronyls can be classified as mixed covalent/ionic interactions. As pointed out in a previous study,[29] this behavior is in contrast with that observed for the C−N bonds in cyanide/isocyanide compounds, which exhibits clear characteristics of mainly shared (covalent) interaction: high values of $\rho(r)$, negative values of $\nabla^2\rho(r)$, negative values of $H(r)$, and also relationships between the potential energy density and the kinetic energy density, $V(r)/G(r)$, greater than 2. Thus, although isoelectronic, CN and BO species show important differences in nature.

Concerning the X−B and X−O bonds in the XBO and XOB species we can find a gradual change from sodium to chlorine compounds. The Na−B bond in NaBO and the Na−O bond in NaOB exhibit characteristics of essentially closed-shell (ionic) interactions: very low electronic densities, positive Laplacians. and small, but positive, energy densities. The corresponding bonds in the silicon compounds, SiBO and SiOB, are both of an intermediate nature: low values of $\rho(r)$, positive values of $\nabla^2\rho(r)$, but small negative values of $H(r)$. In this case the bonds can be classified as intermediate between closed-shell and shared interactions. The compounds containing sulfur and phosphorus, with electronegativities not too far from that of boron, exhibit a different behavior depending on the connectivity. Both P−B and S−B bonds in PBO and SBO, respectively, are mainly shared interactions, indicating a predominant covalent bond (even the relationship between $V(r)/G(r)$ is greater than 2). However, both P−O and S−O bonds in POB and SOB show characteristics of intermediate interactions (positive Laplacian but negative energy density). Finally, for chlorine compounds both Cl−B and Cl−O correspond mainly to shared interactions.

The molecular graphs and contour maps of the Laplacian of the electronic charge density, $\nabla^2\rho$, for XBO/XOB species, calculated at the CCSD/aug-cc-pVTZ level of theory, are provided as Supporting Information (Figure S1). In that figure it can be seen the change in the interaction between the second-row atom and the B atom for XBO isomers, from a main closed-shell interaction (Na) to a mainly shared one (Cl). It is also worth mentioning that the nonlinear species for [NaBO] shows only a Na−O bond critical point, supporting the description of this species as an L-shaped structure.

4. CONCLUSIONS

A computational study of the monoboronyl compounds of the second-row elements Na, Si, P, S, and Cl has been carried out. It has been shown that [NaBO] exhibits a rather flat PES. Three minima were characterized, linear NaBO, linear NaOB, and an L-shaped structure with a ∠NaOB angle of 92.3°. The NaBO isomer and the L-shaped structure are nearly isoenergetic, the former lying slightly lower in energy (0.26 kcal/mol) at the highest level of theory. Linear NaOB is located 2.11 kcal/mol above linear NaBO. The barrier for the conversion of the L-shaped structure into linear NaBO is about 5.1 kcal/mol. Therefore, it seems that both species could be potential targets for experimental detection. In the case of silicon monoboronyl only two minima, linear SiBO and linear SiOB, are found. SiOB lies about 13 kcal/mol above SiOB, and the barrier for the isomerization of SiOB into SiBO is

DOI: 10.1021/acs.jpca.7b10482
J. Phys. Chem. A XXXX, XXX, XXX−XXX

estimated to be 11.4 kcal/mol. Although SiBO seems the main target for experimental observation, SiOB should not be discarded.

For the rest of second-row monoboronyls the preference for the XBO arrangement is much clearer. In fact, for monoboronyls of phosphorus, sulfur, and chlorine the linear XOB species is shown to be a transition state, because in all cases imaginary frequencies are found for the degenerate bending mode. Nonlinear minima are found in these cases, although all of them lying quite high in energy above linear XBO: 46.45 (P), 80.96 (S), and 119.5 (Cl) kcal/mol, respectively. Furthermore, in all cases small barriers for their conversion into the XBO isomer are found, suggesting that quite likely the linear XBO isomer should be the main experimental target.

Dissociation energies of monoboronyls tend to increase when moving from left to right of the second row. Linear XBOs, which are the most stable isomers for the different [XBO] species, have moderate dissociation energies for Na (69.8 kcal/mol), Si (79.24 kcal/mol), and P (78.97 kcal/mol). However, relatively large dissociation energies are found for SBO (97.55 kcal/mol) and ClBO (118.98 kcal/mol).

An analysis of the bonding situation for second-row monoboronyls has also been carried out, emphasizing the different characteristics of the X−B and X−O bonds along the second-row.

Compared to their isoelectronic [XCN] analogues, second-row monoboronyls exhibit similar behaviors, favoring the XBO species over the XOB ones, and this preference is more marked as one moves from Na to Cl. The main difference resides in the stability difference between both types of species. The energy differences found between the XBO/XOB isomers are much larger than those found for the isoelectronic XCN/XNC species.

It is hoped that the structural data provided by the theoretical calculations for the most stable structures of second-row monoboronyls might help in a possible experimental observation.

■ ASSOCIATED CONTENT

Supporting Information

The Supporting Information is available free of charge on the ACS Publications website at DOI: 10.1021/acs.jpca.7b10482.

Table S1, T1 diagnostic values in the CCSD/aug-cc-pVTZ calculations for the different minima of [XBO] systems; Table S2, corre-valence and relativistic corrections for the geometrical parameters of the different linear XBO and XOB species.; Table S3, spin−orbit corrections for different minima of the [XBO] systems; Figure S1, molecular graphs and contour maps of the Laplacian of the electronic charge density, $\nabla^2\rho$, for XBO/XOB species (PDF)

■ AUTHOR INFORMATION

Corresponding Author

*A. Largo. Electronic mail: alargo@qf.uva.es.

ORCID

Víctor M. Rayón: 0000-0003-1973-1084

Carmen Barrientos: 0000-0003-0078-7379

Antonio Largo: 0000-0003-4959-4850

Notes

The authors declare no competing financial interest.

■ REFERENCES

(1) Ehlers, A. W.; Baerends, E. J.; Bickelhaupt, F. M.; Radius, U. Alternatives to the CO Ligand: Coordination of the Isolobal Analogues BF, BNH_2, $BN(CH_3)_2$, and BO^- in Mono- and Binuclear First-Row Transition Metal Complexes. *Chem. - Eur. J.* **1998**, *4*, 210−221.

(2) Zhai, H. J.; Chen, Q.; Bai, H.; Li, S. D.; Wang, L. S. Boronyl Chemistry: The BO Group as a New Ligand in Gas-Phase Clusters and Synthetic Compounds. *Acc. Chem. Res.* **2014**, *47*, 2435−2445.

(3) Braunschweig, H.; Radacki, K.; Schneider, A. Oxoboryl Complexes: Boron-Oxygen Triple Bonds Stabilized in the Coordination Sphere of Platinum. *Science* **2010**, *328*, 345−347.

(4) Braunschweig, H.; Radacki, K.; Schneider, A. Reactivity of an Oxoboryl Complex toward Fluorinated Aryl Boron Reagents. *Chem. Commun.* **2010**, *46*, 6473−6475.

(5) Kaneko, T.; Takao, T.; Suzuki, H. A Triruthenium Complex Capped by a Triple Bridging Oxoboryl Ligand. *Angew. Chem., Int. Ed.* **2013**, *52*, 11884−11887.

(6) Zubarev, D. Y.; Boldyrev, A. I.; Li, J.; Zhai, H. J.; Wang, L. S. On the Chemical Bonding of Gold in Auro-Boron Oxide Clusters Au_nBO^- (n = 1−3). *J. Phys. Chem. A* **2007**, *111*, 1648−1658.

(7) Miao, C. Q.; Lu, H. G.; Li, S. D. Covalent Bonding in $Au(BO)_2^-$ and $Au(BS)_2^-$. *J. Cluster Sci.* **2013**, *24*, 233−241.

(8) Zhai, H. J.; Li, S. D.; Wang, L. S. Boronyls as Key Structural Units in Boron Oxide clusters: $B(BO)_2^-$ and $B(BO)_3^-$. *J. Am. Chem. Soc.* **2007**, *129*, 9254−9255.

(9) Li, S. D.; Zhai, H. J.; Wang, L. S. $B_2(BO)_2^-$ - Diboronyl diborene: A Linear Molecule with a Triple Boron-Boron Bond. *J. Am. Chem. Soc.* **2008**, *130*, 2573−2579.

(10) Bock, H.; Cederbaum, L. S.; von Niessen, W.; Paetzold, P.; Rosmus, P.; Solouki, B. Gas-Phase Reactions 0.70. Methylboron Oxide, H_3C-B═O. *Angew. Chem., Int. Ed. Engl.* **1989**, *28*, 88−90.

(11) Lanzisera, D. V.; Andrews, L. Reactions of Laser-Ablated Boron Atoms with Methanol. Infrared Spectrta and ab Initio Calculations of CH_3BO, CH_2BOH, and CH_2BO in Solid Argon. *J. Phys. Chem. A* **1997**, *101*, 1482−1487.

(12) Kaiser, R. I.; Balucani, N. Exploring the Gas Phse Synthesis of the Elusive Class of Boronyls and the Mechanism of Boronyl Radical Reactions under Single Collision Conditions. *Acc. Chem. Res.* **2017**, *50*, 1154−1162.

(13) Chang, Y.; Li, Q. S.; Xie, Y.; King, R. B. Prospects for Three-Rlectron Donor Boronyl (BO) Ligands and Dioxodiborene (B_2O_2) Ligands as Bridging Groups in Binuclear Iron Carbonyl Derivatives. *Inorg. Chem.* **2012**, *51*, 8904−8915.

(14) Chang, Y.; Li, Q. S.; Xie, Y.; King, R. B.; Schaefer, H. F. Binuclear Iron Boronyl Carbonyls Isoelectronic with the Well-Known Decacarbonyldimanganese. *New J. Chem.* **2012**, *36*, 1022−1030.

(15) Gong, X.; Zhu, L. S.; Yang, J.; Gao, X.; Xie, Y.; King, R. B. Iron Carbonyl Thioboronyls: Effect of Substitution of Sulfur for Oxygen in the Viability of Binuclear Complexes Toward Dissociation Reactions. *Theor. Chem. Acc.* **2014**, *133*, 1585.

(16) Zhang, Z.; Pu, L.; Li, Q.; King, R. B. The Siliconyl, Boronyl, and Iminoboryl ligands as Analogues of the Ell-known Carbonyl Ligand: Predicted Reactivity Towards Dipolar Cyclooligomerization in Iron/Cobalt Carbonyl Complexes. *RSC Adv.* **2015**, *5*, 35558−35563.

(17) Duan, L.; Peng, B.; Luo, Q.; Li, Q.; Xie, Y.; King, R. B. Diverse Bonding Modes and Coupling Reactions of the Boronyl Ligand in Binuclear Cyclopentadienyl Cobalt Derivatives: Analogues with Isoelectronic Binuclear Cyclopentadienyliron Carbonyls. *J. Organomet. Chem.* **2014**, *751*, 662−669.

(18) Gong, X.; Li, Q. S.; Xie, Y.; King, R. B.; Schaefer, H. F. Boronyl Ligand as a Member of the Isoelectronic Series $BO^- \rightarrow CO \rightarrow NO^+$: Viable Cobalt Carbonyl Boronyl Derivatives? *Inorg. Chem.* **2010**, *49*, 10820−10832.

DOI: 10.1021/acs.jpca.7b10482
J. Phys. Chem. A XXXX, XXX, XXX−XXX

(19) Chang, Y.; Li, Q. S.; Xie, Y.; King, R. B. Major Differences between the Binuclear Manganese Boronyl Carbonyl $Mn_2(BO)_2(CO)_9$ and its Isoelectronic Chromium Carbonyl Analogue $Cr_2(CO)_{11}$. *J. Phys. Chem. A* **2013**, *117*, 2260−2268.
(20) Zhao, H.; Peng, A.; Zhang, X.; Li, Q. S.; King, R. B. The Verdsatility of the Boronyl (BO) and Fluoroborylene (BF) Ligands in Binuclear CyclopentadienylpalladiumChemistry. *Inorg. Chim. Acta* **2013**, *406*, 285−292.
(21) Zhang, S.; Zhang, X.; Li, Q. S.; King, R. B. The Versatility of the Boronyl Ligand in Binuclear Cyclopentadienylrhodium Derivatives. *Polyhedron* **2013**, *56*, 24−33.
(22) Zeng, G.; Sakaki, S. Theoretical Study on the Transition-Metal Oxoboryl Complex: M-BO Bonding Nature, Mechanism of the Formation Reaction, and Prediction of a New Oxoboryl Complex. *Inorg. Chem.* **2012**, *51*, 4597−4605.
(23) Zhang, Z.; Pu, L.; Li, Q. S.; King, R. B. Controlling the Reactivity of the Boronyl Group in Platinum Complexes toward Cyclodimerization: A Theoretical Survey. *Inorg. Chem.* **2015**, *54*, 10281−10286.
(24) Papakondylis, A.; Mavridis, A. Structure and Bonding of the Polytopic Molecule Li[BO]. A Theoretical Investigation. *J. Phys. Chem. A* **2001**, *105*, 7106−7110.
(25) Papakondylis, A.; Mavridis, A. Electronic and Geometrical Structure of the Sc[BO]+ Cation. An Ab Initio Investigation. *J. Phys. Chem. A* **1999**, *103*, 9359−9363.
(26) Fuentealba, P. On the Ground-State Structure of XBO (X = Li, Na, and K) Molecules. *Chem. Phys. Lett.* **1999**, *301*, 59−63.
(27) Nguyen, M. T.; Groarke, P. J.; Ha, T. K. Calculated Properties of some Oxoborons RBO (R = H, F, Cl, and CH_3) and their Higher Energy Isomers ROB. *Mol. Phys.* **1992**, *75*, 1105−1121.
(28) Moon, J.; Kim, J. Theoretical Investigation on the Molecular Properties of PtBO and PdBO. *Comput. Theor. Chem.* **2017**, *1108*, 23−28.
(29) Vega-Vega, A.; Barrientos, C.; Largo, A. Metallic Monoboronyl Compounds: Prediction of their Structure and Comparison with the Cyanide Analogues. *J. Comput. Chem.* **2017**, *38*, 807−815.
(30) Dunning, T. H. Gaussian-Basis Sets for Use in Correlated Molecular Calculations 0.1. The Atoms Boron Through Neon and Hydrogen. *J. Chem. Phys.* **1989**, *90*, 1007−1023.
(31) Woon, D. E.; Dunning, T. H. Gaussian-Basis Sets for Use in Correlated Molecular Calculations. 3. The Atoms Aluminum through Argon. *J. Chem. Phys.* **1993**, *98*, 1358−1371.
(32) Raghavachari, K.; Trucks, G. W.; Pople, J. A.; Head-Gordon, M. A. 5th-Order Perturbation Comparison of Electron Correlation Theories. *Chem. Phys. Lett.* **1989**, *157*, 479−483.
(33) Lee, T. J.; Taylor, P. R. A diagnostic for Determining the Quality of Single-reference Electron Correlation Methods. *Int. J. Quantum Chem.* **1989**, *36*, 199−207.
(34) Heckert, M.; Kallay, M.; Gauss, J. Molecular Equilibrium Geometries Based on Coupled-Cluster Calculations Including Quadruple Excitations. *Mol. Phys.* **2005**, *103*, 2109−2115.
(35) Heckert, M.; Kallay, M.; Tew, D. P.; Klopper, W.; Gauss, J. Basis-set extrapolation Techniques for the Accurate Calculation of Molecular Equilibrium Geometries Using Coupled-Cluster Theory. *J. Chem. Phys.* **2006**, *125*, 044108.
(36) Huang, X. C.; Lee, T. J. A Procedure for Computing Accurate ab Initio Quartic Force Fields: Application to HO_2^+ and H_2O. *J. Chem. Phys.* **2008**, *129*, 044312.
(37) Helgaker, T.; Klopper, W.; Koch, H.; Noga, J. Basis-set Convergence of Correlated Calculations on Water. *J. Chem. Phys.* **1997**, *106*, 9639−9646.
(38) Peterson, K. A.; Dunning, T. H. Accurate Correlation Consistent Basis Sets for Molecular Core-Valence Correlation Effects: The Second Row Atoms Al-Ar, and the First Row Atoms B-Ne Revisited. *J. Chem. Phys.* **2002**, *117*, 10548−10560.
(39) Hess, B. A. Applicability of the No-Pair Equation with Free-Particle Projection Operators to Atomic and Molecular-Structure Calculations. *Phys. Rev. A: At., Mol., Opt. Phys.* **1985**, *32*, 756−763.
(40) Hess, B. A. Relativistic Electronic-Structure Calculations Employing a 2-Component No-Pair Formalism with External-Field Projection Operators. *Phys. Rev. A: At., Mol., Opt. Phys.* **1986**, *33*, 3742−3748.
(41) Jansen, G.; Hess, B. A. Revision of the Douglas-Kroll transformation. *Phys. Rev. A: At., Mol., Opt. Phys.* **1989**, *39*, 6016−6017.
(42) Frisch, M. J.; Trucks, G. W.; Schlegel, H. B.; Scuseria, G. E.; Robb, M. A.; Cheeseman, J. R.; Scalmani, G.; Barone, V.; Mennucci, B.; Petersson, G. A.; et al. *Gaussian 09*; Gaussian, Inc.: Wallingford, CT, 2010.
(43) Stanton, J. F.; Gauss, J.; Harding, M. E.; Szalay, P. G. *CFOUR*, a quantum chemical program package, 2013.
(44) Bader, R. W. F. *Atoms in Molecules: A Quantum Theory*; Clarendon Press: New York, 1990.
(45) Keith, T. A., *AIMAll*, version 13.11.04, Professional; TK Gristmill Software: Overland Park, KS, 2013.
(46) Clementi, E.; Kistenmacher, H.; Popkie, H. Study of Electronic-Structure of Molecules. 18. Interaction between a Lithium Atom and a Cyano Group as an Example of a Polytopic Bond. *J. Chem. Phys.* **1973**, *58*, 2460−2466.
(47) Marsden, C. J. Ab Initio Correlated Potential-Energy Surfaces for Monomeric Sodium and Potassium Cyanides. *J. Chem. Phys.* **1982**, *76*, 6451−6452.
(48) Senent, M. L.; Dumouchel, F.; Lique, F. Cyanide/Isocyanide Abundances in the Interstellar Medium − I. Theoretical Spectroscopic Characterization. *Mon. Not. R. Astron. Soc.* **2012**, *420*, 1188−1194.
(49) Turner, B. E.; Steimle, T. C.; Meerts, L. Detection of Sodium Cyanide (NaCN) in IRC-10216. *Astrophys. J.* **1994**, *426*, L97−L100.
(50) Halfen, D. T.; Ziurys, L. M. Millimeter and Submillimeter Rest Frequencies for NaCN (X^1A'): a Remarkably Abundant Circumstellar Molecule. *Astrophys. J.* **2011**, *730*, 107.
(51) Largo-Cabrerizo, A. A Theoretical Study of the SiCN Radical. *Chem. Phys. Lett.* **1988**, *147*, 95−98.
(52) Richardson, N. A.; Yamaguchi, Y.; Schaefer, H. F. Isomerization of the Interstellar Molecule Silicon Cyanide to Silicon Isocyanide through Two Transition States. *J. Chem. Phys.* **2003**, *119*, 12946−12955.
(53) Apponi, A. J.; McCarthy, M. C.; Gottlieb, C. A.; Thaddeus, P. The Radio Spectra of SiCCH, SiCN, and SiNC. *Astrophys. J.* **2000**, *536*, L55−L58.
(54) McCarthy, M. C.; Apponi, A. J.; Gottlieb, C. A.; Thaddeus, P. Rotational Spectra of SiCN, SiNC, and the SiCnH (n = 2, 4−6) Radicals. *J. Chem. Phys.* **2001**, *115*, 870−877.
(55) Guélin, M.; Muller, S.; Cernicharo, J.; Apponi, A. J.; McCarthy, M. C.; Gottlieb, C. A.; Thaddeus, P. Astronomical Detection of the Free Radical SiCN. *Astron. Astrophys.* **2000**, *363*, L9−L12.
(56) Guélin, M.; Muller, S.; Cernicharo, J.; McCarthy, M. C.; Thaddeus, P. Detection of the SiNC Radical in IRC+10216. *Astron. Astrophys.* **2004**, *426*, L49−L52.
(57) Largo, A.; Barrientos, C. Theoretical Studies of Possible Processes for the Interstellar Production of Phosphorus Compounds. Reaction of P^+ with HCN and Protonation of CNP Compounds. *J. Phys. Chem.* **1991**, *95*, 9864−9868.
(58) El-Yazal, J.; Martin, J. M. L.; François, J. P. Structure and Vibrations of the C_2P and CNP Radicals and their Cations Using Density Functional and Coupled Cluster Theories. *J. Phys. Chem. A* **1997**, *101*, 8319−8326.
(59) Halfen, D. T.; Sun, M.; Clouthier, D. J.; Ziurys, L. M. The Microwave and Millimeter Rotational Spectra of the PCN radical ($X^3\Sigma^-$). *J. Chem. Phys.* **2012**, *136*, 144312.
(60) Diehr, M.; Chambaud, G.; Werner, H.-J. Theoretical Study of the Dissociation and Isomerization of NCS. *Z. Phys. Chem.* **2003**, *217*, 255−264.
(61) Fitzgerald, M.; Bowie, J. H. The Generation of the Thiocyanate Radical and Cation from the Thiocyanate Anion $[SCN]^-$ in the Gas Phase. The Rearrangements of Neutral and Cationic SCN. A Joint

DOI: 10.1021/acs.jpca.7b10482
J. Phys. Chem. A XXXX, XXX, XXX−XXX

Experimental and Theoretical Study. *J. Phys. Chem. A* **2004**, *108*, 3668−3674.
(62) Snelson, A. Infrared Matrix Isolation Spectra of OBCl AND OBBr. *High Temp. Sci.* **1972**, *4*, 318.
(63) Kawaguchi, K.; Endo, Y.; Hirota, E. Infrared Diode Laser and Microwave Spectroscopy of an Unstable Molecule: ClBO. *J. Mol. Spectrosc.* **1982**, *93*, 381−388.
(64) Hunt, N. T.; Röpcke, J.; Davies, P. B. Infrared Diode Laser Spectrum of the ν_1 Fundamental Band of ClBO. *J. Mol. Spectrosc.* **2000**, *204*, 120−124.
(65) Gatehouse, B.; Müller, H. S. P.; Gerry, M. C. L. Hyperfine Constants and Nuclear Shieldings from the Microwave Spectra of FBO, ClBO, and FBS. *J. Mol. Spectrosc.* **1998**, *190*, 157−167.
(66) Reed, A. E.; Curtiss, L. A.; Weinhold, F. Intermolecular Interactions from a Natural Bond Orbital, Donor-Acceptor Viewpoint. *Chem. Rev.* **1988**, *88*, 899−926.
(67) Brand, J.; Braunschweig, H.; Sen, S. S. B═B and B E (E = N and O) Multiple Bonds in the Coordination Sphere of Late Transition Metals. *Acc. Chem. Res.* **2014**, *47*, 180−191.
(68) Harcourt, D. R. In *Pauling's Legacy: Modern Modelling of the Chemical Bond*; Maksic, Z. B., Orville-Thomas, W. J., Eds.; Elsevier: Amsterdam, 1999.
(69) Sizova, O. V.; Skripnikov, L. V.; Sokolov, A. Y. Symmetry Decomposition of Quantum Chemical Bond Orders. *J. Mol. Struct.: THEOCHEM* **2008**, *870*, 1−9.
(70) Hathwar, V. R.; Paul, A. K.; Natarajan, S.; Row, T. N. G. Charge Density Analysis of a Pentaborate Ion in an Ammonium Borate: Toward the Understanding of Topological Features in Borate Minerals. J. *J. Phys. Chem. A* **2011**, *115*, 12818−12825.

DOI: 10.1021/acs.jpca.7b10482
J. Phys. Chem. A XXXX, XXX, XXX−XXX